Generation and Evaluation of Monodisperse Sodium Chloride and Oleic Acid Nanoparticles

Tzu Ming Chen, Hung Min Chein*

Energy & Environment Research Laboratories,
Industrial Technology Research Institute, Chutung, Hsinchu 310, Taiwan

Abstract

Nanomaterial application has been recognized as a most important future development for nanomaterial production industries. However, harmful toxic pollutants, especially nanoparticles, could also be produced in the process. Therefore, there is a need to evaluate control technologies by generating monodisperse nanoparticles for experimental purposes. In this research project, atomization and vaporization-condensation technologies were applied to generate solid (NaCl) and liquid (oleic acid) polydisperse particles. A differential mobility analyzer (DMA) was utilized to segregate and produce test nanoparticles. In the generation of polydisperse particles, the geometric standard deviation (GSD) and total number concentration (NC) of NaCl particles segregated from various $NaCl_{(aq)}$ concentration were 1.59–1.89 and $8.47 \times 10^5 – 4.2 \times 10^6$ #/cm^3. Results show that as $NaCl_{(aq)}$ concentration increases, GSD also increase. However, there is a logarithm relation ($y = 2 \times 10^6 \text{Ln}(x) + 2 \times 10^6$) between $NaCl_{(aq)}$ concentration and NC. For polydisperse oleic acid particles, GSDs and NC of particles segregated from various furnace temperatures are 1.43–1.65 and $7.12 \times 10^5 – 5.35 \times 10^6$ #/cm^3, respectively. GSDs and NC of oleic acid particles generated from various carrier gas flow are 1.41–1.63 and $7.31 \times 10^6 – 9.42 \times 10^6$ #/cm^3, respectively. Furnace temperature and NC are a logarithm relation. Carrier gas flow and NC is a polynomial function. GSD varies as furnace temperature and carrier gas flow increase. Monodisperse nanoparticles were successfully generated from the atomization of 0.5% $NaCl_{(aq)}$ and oleic acid. The GSD, count median diameter (CMD), and total number concentration (NC) NaCl particles segregated from various DMA voltages were 1.04 – 1.08 and 8.33 nm – 128 nm, and $9.89 \times 10^2 – 2.67 \times 10^5$ #/cm^3, respectively. The GSD, CMD, and total NC of monodisperse oleic acid particles produced from various DMA voltages were 1.04 – 1.06, 8.9 nm – 92.5 nm, and $2.4 \times 10^4 – 7.6 \times 10^5$ #/cm^3, respectively.

* Corresponding author. Tel: +886-3-5913853; Fax: +886-3-5820378;
E-*mail address*: hmchein@itri.org.tw

INTRODUCTION

Nanomaterial application is acknowledged as one of the most important industries in the 21st century and is expected to create great economic value in almost every aspect of human life. However, nanoindustries may also produce and release toxic pollutants into the environment, especially nanoparticles. Thus, research and development of nanoparticle control technologies and equipment will be very important in finding ways to reduce harmful emissions. But before developing control technology and equipment, it will be necessary to generate and evaluate test nanoparticles under experimental conditions. Test nanoparticles can be applied to evaluate control instruments, personal protective equipment, and samplers. The generation of test nanoparticles is also important for nanoparticle instrumentation development and calibration. Test nanoparticles can also be used in inhalation research on humans and animals exposed to harmful nanoparticles. The geometric standard deviation (GSD) of general test particles is less than 1.10. This study required sizes less than 100 nm, and GSD less than 1.05.

Many mechanisms (Takahashi, 1989) generate polydiperse aerosols or particles. Spray, which employ raw materials including DOP, oil, salt, tetramethyl blue, and PSL, is a common way to generate solid and liquid particles. Atomizer is considered an aerosol generator of high stability (Liu and Lee, 1975). Vaporization-condensation technology is another common approach, which usually employs furnaces to generate aerosols. This method can generate many kinds of aerosols, including liquid (oleic acid, DOP, oil, etc.), metal particles (Deppert *et al*., 1996) and compounds (Kruis *et al.*, 1996). Powder dispersion can produce solid particles by dust feeder. Chemical reaction mechanisms can generate complex compound particles by plasma reactors, or flame reactors; for example, $Fe(CO)_5$ and $SiO_2(CH_3)_6$ (Zachariah *et al.*, 1995). However, these reactors usually need high reaction temperatures (Kruis *et al.*, 1998).

There are two usual ways of producing these monodisperse particles using aerosol technology. One is to produce polydisperse nanoparticles, and consequently, classify the desirable particle sizes by differential mobility analyzer (DMA). The classified monodisperse particles are then measured using a second DMA that is scanned through voltages. This method is called Tandem Differential Mobility Analyzer (TDMA; Rader and McMurry, 1986). The other way is to generate monodisperse particles directly, using aerosol generation techniques. Table 1 is a list of commercial products which can directly generate monodisperse particles. The Vibrating Orifice Aerosol Generator (Remiarz *et al.*, 1982) has the smallest GSD (1.01), but it cannot generate nano-scale particles. Condensation monodisperse aerosol generator (TSI), condensation aerosol generator SLG 270 (Topas GmbH), and the new Sinclair-LaMer aerosol generator MAG-3000 (Altmann and Peters, 1992) can produce smaller particles; however, its GSD is too high and produces particles larger than 100 nm. Electrospray aerosol generator (Chen *et al.*, 1995) can

produce high concentrations of monodisperse nanoparticles, but its GSD is still higher than 1.05.

The purpose of this research is to generate NaCl and oleic acid nanoparticles with count median diameter (CMD) between 10 and 100 nm, and GSD less than or equal to 1.05. The total particle number concentration (NC) needs to be high enough for the above-described applications.

Table 1. A list of commercial monodisperse particle generators.

Name of commercial product	Size range	GSD	Particle Type	Carrier gas	Application technology
Vibrating Orifice Aerosol Generator (TSI) http://www.tsi.com/	1–200 μm	< 1.01	Oil and solids soluble in water or alcohol.	Air	Spray
Condensation Aerosol Generator SLG 270 (Topas GmbH) http://www.topas-gmbh.de	0.1–12 μm	< 1.15	*Liquid*: DEHS, Engine oil 15W40, Emery 3004 *Solid*: Carnauba Wax, Stearic Acid, Paraffins	N_2	Spray/ Condensation
Condensation Monodisperse Aerosol Generator (TSI) http://www.tsi.com/	0.1–0.5 μm 0.5–8 μm	< 1.25 < 1.10	Solid: Carnauba wax, paraffin, or stearic acid. Liquid: DES, DOP, etc.	N_2	Spray
New Sinclair-LaMer aerosol generator MAG-3000 (PALAS) http://www.palas.de	.5–8 μm	< 1.2	*Liquid*: DEHS, paraffin oil *Solid*: saline solution	N_2	Spray
Electrospray Aerosol Generator (TSI) http://www.tsi.com/	3–100 nm	1.1	Water-soluble, nonvolatile solids and liquids.	CO_2	Spray

METHODOLOGY

For NaCl polydisperse nanoparticle generation, we chose spray method to generate NaCl particles. A Constant Output Atomizer (COA), a commercial product driven by compressed air, was used to produce the CMD of NaCl particle, which is normally between 20 and 300 nm, and GSD, which is around 1.9 (TSI, 2002). We applied vaporization-condensation technology to generate oleic acid polydisperse droplet generation. This method employs a tube furnace to evaporate the oleic acid liquid and form a saturated vapor, which was subsequently cooled and condensed into aerosols. Its GSD is around 1.2–1.4 because the aerosol's diameter is quite uniform when vapor molecules condense on the nuclei (Hinds, 1999).

Scanning Mobility Particle Sizer (SMPS) was utilized to monitor the particle NC and size distribution. The SMPS consists of electrostatic classifier (EC) and ultrafine condensation particle counter (UCPC). Another DMA was employed for generating monodisperse particles. The EC

utilized electrical mobility to classify and collect particles by adjusting the DMA's voltage, while the UCPC enlarged the classified aerosol by saturated alcohol vapor. The particle-laden vapor flowed through a cold tube to create the level of super saturation required for particle growth. Since each nucleus grows to a droplet, the number concentration of droplets and nuclei remain the same. The number concentration of droplets was then measured by an optical counter (Baron and Willeke, 2001).

The polydisperse aerosol was passed through an ^{85}Kr neutralizer (TSI Model 3077) in order to obtain a well-defined Boltzmann equilibrium charge distribution of the particles. For particles less than 100 nm in diameter, this approach produces an aerosol in which the fraction of charged particles decreases with decreasing size. Only a small fraction of the particles in this size range carry more than one charge (Flagan, 1998). When the particle size is larger than 100 nm, however, the fraction of multiple-charged particles dramatically rises so that particles of several sizes will have the same mobility.

In this study, the main purpose was to generate nanoparticles with CMD between 10 and 100 nm. It is difficult to put more than one charge on small particles. Therefore, we assume all particles are single charge. For avoiding the issue of multiple charge of larger particles, we use a precut impactor to remove particles larger than the largest size nominally being classified with the DMA. The set-up diagrams of generation are shown in Figs. 1A and 1B (Chen and Chein, 2003).

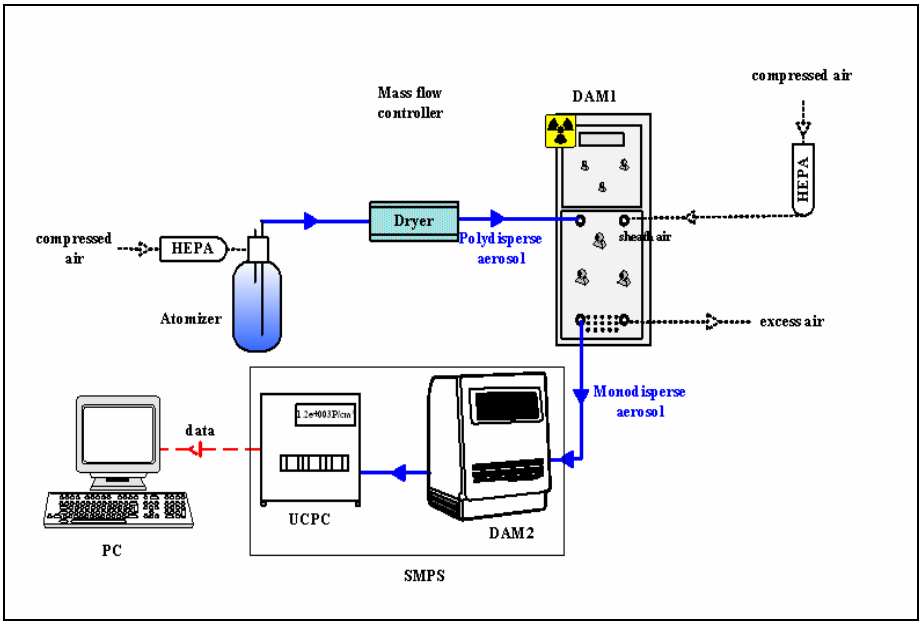

Fig. 1A. Generation system of NaCl nanoparticles.

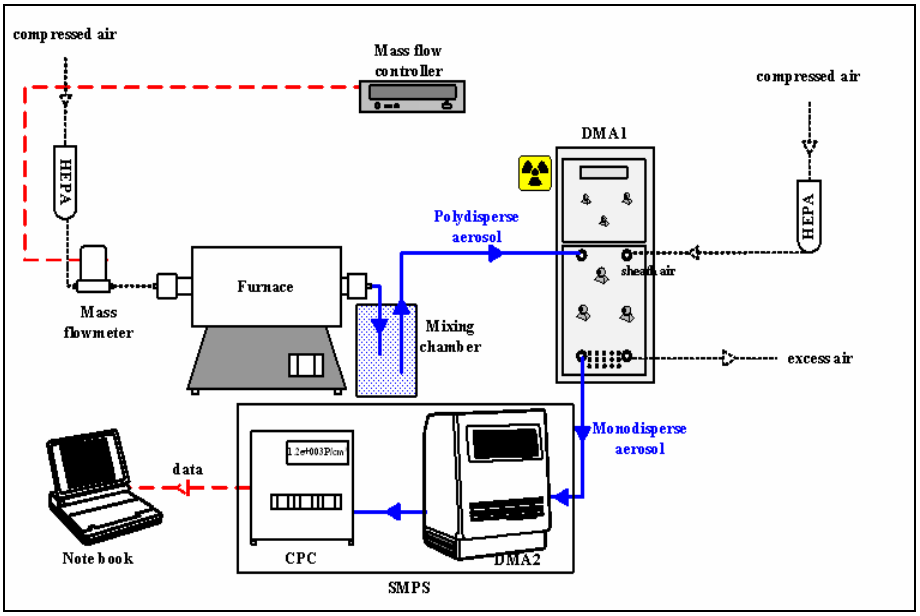

Fig. 1B. Generation system of oleic acid nanodroplets.

Table 2. The regression equations of $NaCl_{(aq)}$ concentration in GSD and NC.

Regression factors	Regression equation	R^2
$NaCl_{(aq)}$ conc. and GSD	$y = 0.0678\ x + 1.5373$	0.86
$NaCl_{(aq)}$ conc. and CMD	$y = 32.202\ x - 27.455$	0.91
$NaCl_{(aq)}$ conc. and NC	$y = 2 \times 10^6 Ln(x) + 2 \times 10^6 Ln$	0.73

RESULTS

Generation of NaCl nanoparticles

NaCl particles were generated using a NaCl solution with different concentrations. Fig. 2 shows size distributions of particles generated from 0.5% $NaCl_{(aq)}$ and 0.01% $NaCl_{(aq)}$, which were mostly under 100 nm. The number concentration of particles from 0.5% $NaCl_{(aq)}$ (4.2×10^6 #/cm^3) was more than 0.01% $NaCl_{(aq)}$ (3.2×10^6 #/cm^3). On the other hand, 1% (4.17×10^6 #/cm^3), 4% (3.76×10^6 #/cm^3) and 10% $NaCl_{(aq)}$ (3.41×10^6 #/cm^3) generated solid particles mostly larger than 100 nm. Therefore, we chose 0.5% $NaCl_{(aq)}$ to be the source of monodisperse NaCl nanoparticle generation. Table 2 lists regression equations and R^2 of $NaCl_{(aq)}$ concentration in GSD, NC and CMD. Table 3 shows the results of monodisperse nanoparticle generation. The size distributions and NC of the nanoparticles classified by various DMA voltages are also shown

in Table 3.

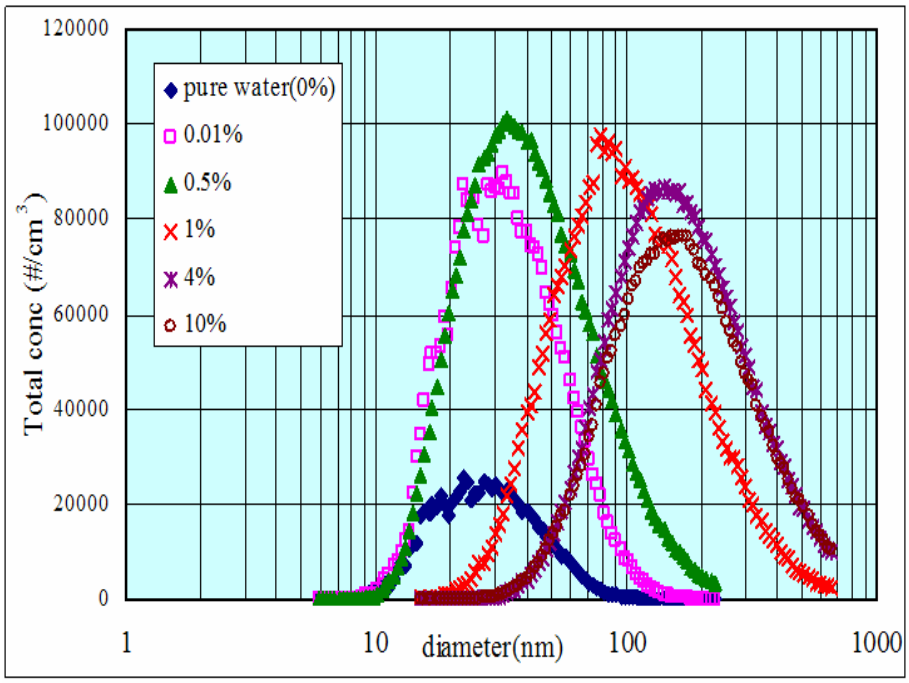

Fig. 2. Size distribution of polydisperse particles produced from $NaCl_{(aq)}$.

Table 3. Results of monodisperse NaCl nanoparticles.

DMA Voltage (V)	Polydisperse	5000	1000	750	400
Median (nm)	38.67	128	74.08	45.05	32.47
GSD	1.79	1.06	1.08	1.05	1.04
Total conc. (#/cm^3)	4.2×10^6	6.27×10^4	1.66×10^5	2.66×10^5	2.76×10^5
DMA Voltage(V)	300	100	50	30	25
Median (nm)	28.03	16.49	11.87	9.33	8.33
GSD	1.04	1.08	1.08	1.05	1.04
Total conc. (#/cm^3)	2.63×10^5	1.22×10^5	1.64×10^4	2.47×10^3	989

UCPC flow: High, SMPS sheath flow rate: 15 L/min, DMA sheath flow rate: 20 L/min

Productions of oleic acid droplets

Generation of droplets via a furnace flow reactor are affected by the furnace temperature, the areas of evaporation, and the flow rate of the carrier gases. In this study, the same container was

used to load identical volumes of oleic acid, so the areas of evaporation were the same. Thus, it was necessary only to find out the best generation temperature and carrier gas before generating monodisperse particles. The distributions of the diameters of oleic acid particles under 200°C, 240°C, 260°C and 280°C (carrier gas flow: 1 L/min) are shown in Fig. 3. The highest particle NC was generated under 200°C (5.35×10^6 #/cm^3), but the diameters of the particles were between 50-200 nm, and most of them were out of desired size range (< 100 nm). The second highest NC was generated below 240°C (3.4×10^6 #/cm^3) and the diameters of the particles were mostly under 100 nm. NCs of 260°C and 280°C were 7.12×10^5 #/cm^3 and 1.67×10^6 #/cm^3.

The size distributions of oleic acid particles under various carrier gas flows (furnace temperature: 240°C) are shown in Fig. 4. The first and second highest NC occurred under 0.6 L/min (5.24×10^6 #/cm^3) and 0.8 L/min (4.85×10^6 #/cm^3) and the sizes of the particles were within the required range. NCs of 0.4 L/min, 1.0 L/min and 1.2 L/min were 1.13×10^6, 3.39×10^6 and 7.31×10^5 #/cm^3. Therefore, we tried 0.7 L/min and its NC was 7.42×10^6 #/cm^3. Thus, the suitable temperature and carrier gas flow for the generation of oleic acid particles chosen were 240°C and 0.7 L/min, respectively.

Table 4 shows regression equations and R^2 of furnace temperature and carrier gas flow rate in GSD, NC and CMD. The distributions of the diameters and NC of monodisperse oleic acid particles classified by DMA under various voltages are shown in Table 5.

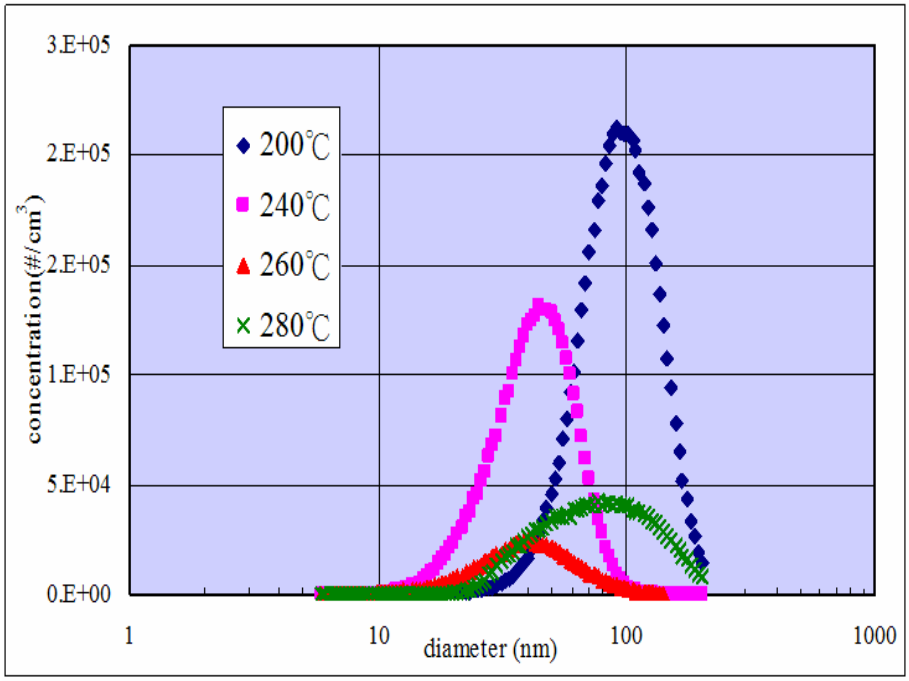

Fig. 3. Size distributions of oleic acid particles under various furnace temperatures.

Table 4. Regression equations of furnace temperature and carrier gas flow rate in GSD and NC.

Regression factors	Regression equation	R^2
Furnace temperature and GSD	$y = 0.076\ x + 1.34$	0.98
Furnace temperature and NC	$y = -3 \times 10^6 Ln(x) + 5 \times 10^6$	0.85
Furnace temperature and CMD	$y = 16.79\ x^2 - 88.318\ x + 143.89$	0.998
Carrier gas flow rate and GSD	$y = 0.051\ x + 1.323$	0.78
Carrier gas flow rate and NC	$y = -10^6\ x^2 + 6 \times 10^6\ x - 3 \times 10^6$	0.95
Carrier gas flow rate and CMD	$y = -13.765\ x + 93.245$	0.82

Table 5. Results of monodisperse oleic acid particles.

Voltage (V)	2300	2000	1700	1400	1100	800
Median (nm)	92.5	85.9	78.4	70.5	61.7	52.1
GSD	1.05	1.04	1.04	1.04	1.04	1.05
Total Conc. (#/cm^3)	2.4×10^4	4.3×10^4	8.2×10^4	1.65×10^5	2.99×10^5	5.0×10^5
Voltage (V)	600	400	200	75	40	25
Median (nm)	44.6	36.1	25.2	15	11	8.9
GSD	1.04	1.05	1.05	1.05	1.05	1.06
Total Conc. (#/cm^3)	6.4×10^5	$7.6 \times 10^{\backslash 5}$	6.2×10^5	3.1×10^5	1.21×10^5	3.0×10^4

UCPC flow – High; SMPS sheath flow rate – 15 L/min; DMA sheath flow rate – 20 L/min; Furnace temperature – 240℃; Carrier gas flow rate – 0.7 L/min.

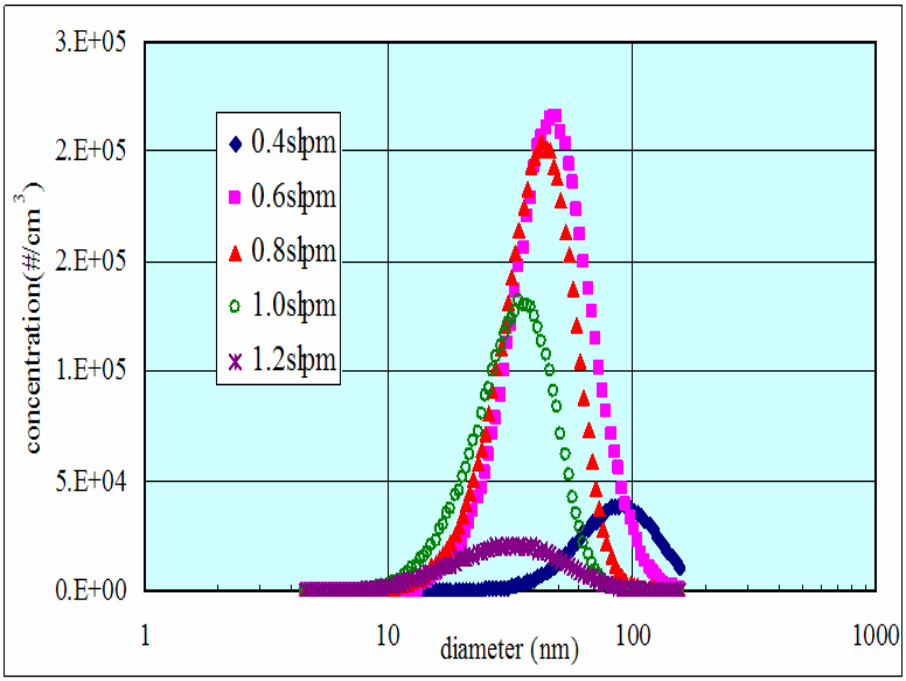

Fig. 4. Size distributions of oleic acid particles under various carrier gas flow of furnace at 240°C.

DISCUSSION

Comparison of experimental and theoretical sizes of NaCl particles

From Table 2, the R^2 is 0.73 between $NaCl_{(aq)}$ concentration and NC which shows that they are considerably well correlated, with a logarithm relation of $y = 2 \times 10^6 Ln(x) + 2 \times 10^6$. There are linear relations between $NaCl_{(aq)}$ concentration and GSD ($y = 0.0678\ x+1.5373$, $R^2 = 0.86$), and between $NaCl_{(aq)}$ concentration and CMD ($y = 32.202\ x-27.455$, $R^2 = 0.91$). The R^2 values show that they are correlated quite well; that is to say, that while $NaCl_{(aq)}$ concentration increases, GSD and CMD also increase in proportion.

Theoretically, the size of generated NaCl particles can also be expressed in the following equation (Hinds, 1999):

$$D_p = D_d \times \sqrt[3]{F_v} \tag{1}$$

Where D_p is particle diameter (nm)

D_d is droplet diameter (nm)

Fv is the volume fraction of solid material.

The diameters of solid particles are influenced by the volume ratio of the solute (NaCl), the solution, and the diameters of the droplets when using atomization method to generate solid

particles. A comparison of the experimental average diameters and theoretical values is shown in Table 6. The theoretical values in the table were calculated by two extreme concentrations. These two theoretical values were calculated by 10% and 0.01% of $NaCl_{(aq)}$ experimental average diameters ($D_{p\text{-}exp}$), and the percent discrepancies were the differences between the experimental and theoretical values. For a theoretical value of 10% $NaCl_{(aq)}$, the experimental and theoretical discrepancies became larger when the concentrations of $NaCl_{(aq)}$ decreased. The highest value of percent discrepancy was −95% for the case of 0.01% $NaCl_{(aq)}$. However, for the theoretical value of 0.01% $NaCl_{(aq)}$, the discrepancies between experimental and theoretical values became smaller as the concentrations of $NaCl_{(aq)}$ decreased. Furthermore, the theoretical diameters were larger than experimental ones, which is different for the case of 10% $NaCl_{(aq)}$.

Table 6. Comparison of experimental and theoretical diameters of polydisperse NaCl particles.

NaCl conc.(%)	0 (pure H_2O)	0.01	0.5	1	4	10
$D_{p\text{-}exp}$ (nm)	26	32	78	97	152	168
$Dp_{(10\%)\text{-}the}$[a] (nm)	0	16	60.6	76	122	168
Percent discrepancy[b] (%)	-	-95%	-29%	-27%	-25%	0%
$Dp_{(0.01\%)\text{-}the}$[c] (nm)	0	32	118	149	237	326
Percent discrepancy (%)	-	0%	34%	35%	36%	38%

[a] D_p (10%) are theoretical values; the D_p was theoretically based on the D_d of the 10% NaCl.

[b] Percent discrepancy = $(D_{p\text{-}the} - D_{p\text{-}exp}) / D_{p\text{-}the}$.

[c] D_p (0.01%) are theoretical values; the D_p was calculated based on the D_d of the 0.01% $NaCl_{(aq)}$.

The discrepancies between the experimental and theoretical results mainly came from the impurities in the solvents (laboratory pure water). Due to the impurity accumulation on the solid particles (Rulison and Flagan, 1994), the particles are larger than expected. The volume of impurity in the water is fixed; for instance (from Table 7, assuming the ratio of the impurity volume to water volume is 1 to 90), the volumes of water and NaCl are 90 cm^3 (1 cm^3 is the impurity) and 10 cm^3, respectively, in 100 cm^3 of 10% $NaCl_{(aq)}$, and the volume ratio of impurity and NaCl is 1 to 10.

In 100 cm^3 of 1% $NaCl_{(aq)}$, the volumes of water and NaCl are 99 cm^3 (1.1 cm^3 is the impurity) and 1 cm^3, respectively, and the volume ratio of impurity to NaCl is 1.1 to 1. When the concentration of NaCl decreases to 0.1%, the volumes of water and NaCl are 99.9 cm^3 (1.11 cm^3 is the impurity) and 0.1 cm^3, respectively, and the volume ratio of impurity and NaCl is 11.1 to 1. From the above, it can be seen that the volume of impurity in the solution decreased as the concentration of NaCl increased. Thus, the effect of impurity can be ignored when the particles

are generated from a high concentration of NaCl solution; in contrast, the effect of impurity becomes greater when the concentration is lower. These are the main reasons for the discrepancies between experimental and theoretical values.

The impurity in the solution will also affect the generation of monodisperse particles. The diameters of impurities range between 6.85 and 202 nm, and their number concentration is about 3.2×10^4 #/cm^3 at most (Fig. 2), so the size limit of monodisperse NaCl particle generation is about 6 nm in these conditions.

Table 7. Ratios of impurities in various concentrations of NaCl solutions.

$NaCl_{(aq)}$ volume concentration (100 cm^3)	10%	1%	0.1%
Laboratory pure water (cm^3) (with impurity)	90	99	99.9
Volume of impurity (cm^3)	1	1.1	1.11
Volume of NaCl (cm^3)	10	1	0.1
Volume ratio of impurity to NaCl	1:10	1.1:1	11.1:1

(Assuming the ratio of the impurity volume to water volume is 1 to 90.)

Comparison of experimental and theoretical sizes of oleic acid droplets

The concentrations and diameters of droplets are affected by the furnace temperature and flow rate of carrier gas. Generally, the concentrations and diameters of oleic acid droplets became higher and larger when the furnace temperature was increased, because the quantity of vapor was increased. However, the experimental data resulted in a logarithm relation ($y = -3 \times 10^6 Ln(x) + 5 \times 10^6$, $R^2 = 0.85$) between furnace temperature and NC. In addition, the experimental relation of furnace temperature and CMD is a polynomial function ($y = 16.79\ x^2 - 88.318\ x + 143.89$, $R^2 = 0.9981$), as shown in Fig. 5. In some cases, the quantity of vapor increased as the carrier gas flow rate increased. However, the vapor concentration decreased and condensation time was affected by fast flow rate conditions (Fig. 6) and the regression relation of carrier gas flow rate and NC is a polynomial function ($y = -10^6\ x^2 + 6 \times 10^6\ x - 3 \times 10^6$). On the GSD, there are linear relations on furnace temperature ($y = 0.076\ x + 1.34$, $R^2 = 0.98$) and carrier gas flow rate ($y = 0.051\ x + 1.323$, and $R^2 = 0.78$), as shown in Table 4. That is to say that GSD of polydisperse oleic acid particles varies as furnace temperature and carrier gas flow rate increase. The relation is also linear between carrier gas flow rate and CMD ($y = -13.765\ x + 93.245$, $R^2 = 0.82$).

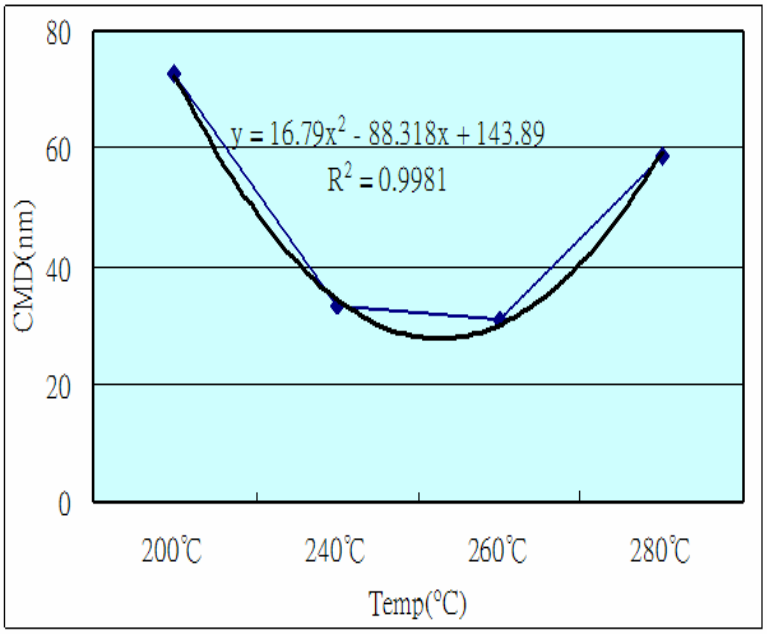

Fig. 5. Regression relation between temperature and CMD for the furnace flow reactor.

In terms of theory; if one can control condensation nuclei, concentration of vapor, and speed of condensation, ignoring the loss of condensation on the tubing wall, the diameter of aerosol can be calculated by Eq. (2). Based on the equation (Hinds, 1999), C_m and N are the main factors affecting diameter:

$$d_d = \left(\frac{6C_m}{\pi \rho_L N} \right)^{1/3} \quad (2)$$

where, d_d: diameter after condensation

C_m: mass concentration of vapor of high boiling liquid

ρ_L: density of high boiling liquid

N: number of condensation nuclei (number of fine particles).

In this study, all of the oleic acid experiments use the same container, so the area of evaporation is the same. The furnace temperature and carrier gas flow rate are the remaining factors that can influence the experiment. Comparisons of experimental data and theoretical values from Eq. (2) of oleic acid particles at different furnace temperatures and carrier gas flow rates are shown in Tables 8 and 9, respectively. The furnace temperatures and carrier gas flow rates showed significant effects on both experimental data and theoretical values. In addition, they showed significant effects on the size distribution of oleic acid droplets, and the discrepancies generally increased as the GSD increased for both cases.

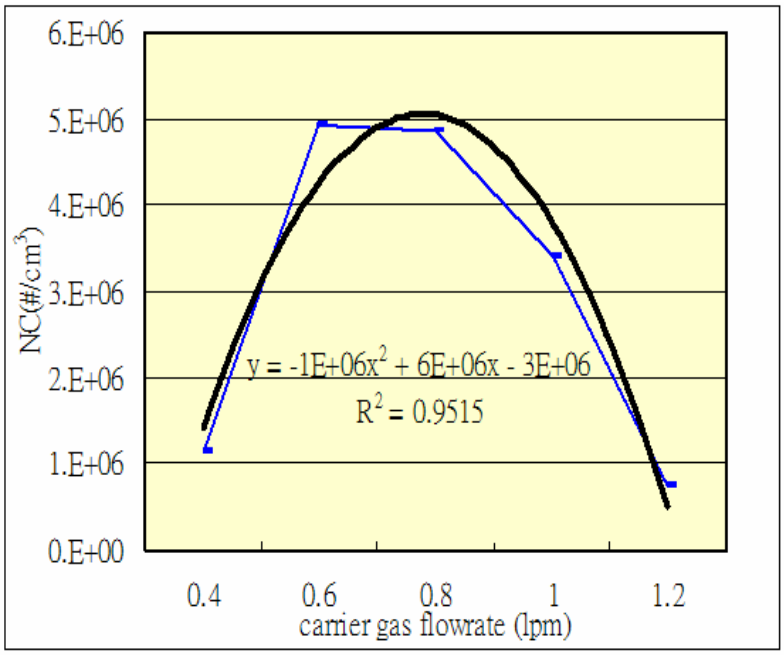

Fig. 6. Relationship between NC and carrier gas flow rate of the furnace flow reactor.

Table 8. Comparison between experimental data and theoretical values of oleic acid droplets at various furnace temperatures.

Furnace temperature (℃)	200	240	260	280
d_d-exp (nm)	72.7	34.7	31.06	58.92
d_d-the (nm)	84.1	39.2	40.5	79
Percent discrepancy* (%)	-16%	-17%	-31%	-34%

* Percent discrepancy = $(d_{d\text{-the}} - d_{d\text{-exp}}) / d_{d\text{-the}}$, Carrier gas flow rate: 1 L/min

When generating monodisperse oleic acid particles, Eq. (2) is used as the foundation of the theoretical calculation. A comparison of experimental data ($d_{d\text{-exp}}$) and theoretical diameters ($d_{d\text{-the}}$) of fine particles is shown in Table 10. All discrepancies were under 1%, except for the discrepancy of 36.1 nm, which was larger than 1.5%. The GSD of monodisperse particles is ≤ 1.06 in Table 5, and one can see that the diameter and uniformity of particles are almost the same when generating from a furnace tube. These results can be verified by the discrepancies in Table 10. The oleic acid particles were generated at the same furnace temperature, carrier gas flow rate, and condensation nuclei. Vapor concentration was also under control, so the experimental diameters of particles had almost no discrepancies from the theoretical values.

Utilization of various voltages of the DMA is the main means of classifying the polydisperse

particles or droplets in this study. The distributions of number concentrations of the particles classified by various voltages are shown in Fig. 3. The highest concentration occurred at 400 V, then the concentrations decreased as the voltages increased further. The main reason for this phenomenon is that the polydisperse distribution is a normal distribution. The two ends of the distribution have fewer numbers of particles. Thus, one can obtain the highest concentration of particles when one classifies at the peak of the normal distribution. The same reasoning also applies for oleic acid monodisperse particles, as verified in Fig. 6.

Based on Eq. (3) (Seola, 2002),

$$D_p = \frac{2 n_p e C_c V L}{3 \mu Q_{sh} \ln \frac{R_2}{R_1}} \quad (3)$$

D_p: diameter of particle (cm)
C_c: slip correction factor
n_p: electron charge of particle
e: 1.6×10^{-19} Coulomb
V: average voltage of the center electrode (volts)
L: distance between monodisperse aerosol exit and polydisperse entrance
μ: viscosity of gas (dyne˙s/cm2)
Q_{sh}: sheath air flow rate
R_1: radius of center electrode
R_2: radius of outer electrode

Table 9. Comparison between experimental data and theoretical values of oleic acid droplets at various carrier gas flow rate.

Carrier gas flow rate (L/min)	0.4	0.6	0.8	1	1.2
d_d-exp (nm)	88.06	54.97	40.88	34.7	33.98
d_d-the (nm)	99.9	63.4	47.0	39.2	42.0
Percent discrepancy (%)	-13%	-15%	-15%	-13%	-24%

Percent discrepancy = $(d_{d\text{-the}} - d_{d\text{-exp}}) / d_{d\text{-the}}$, Furnace temperature: 240℃

When n_p, e, L, μ, Q_{sh}, R_1, and R_2 are fixed, D_p is proportional to V. The black solid line in Fig. 7 is the theoretical relationship between the diameter of monodisperse aerosol and DMA voltage. The circles and squares represent the relationship between the experimental diameter of monodisperse NaCl and oleic acid particles and the voltage of DMA employed, respectively. There are almost no discrepancies between the experimental results and theoretical values; therefore, the results from our laboratory match the theoretical predictions.

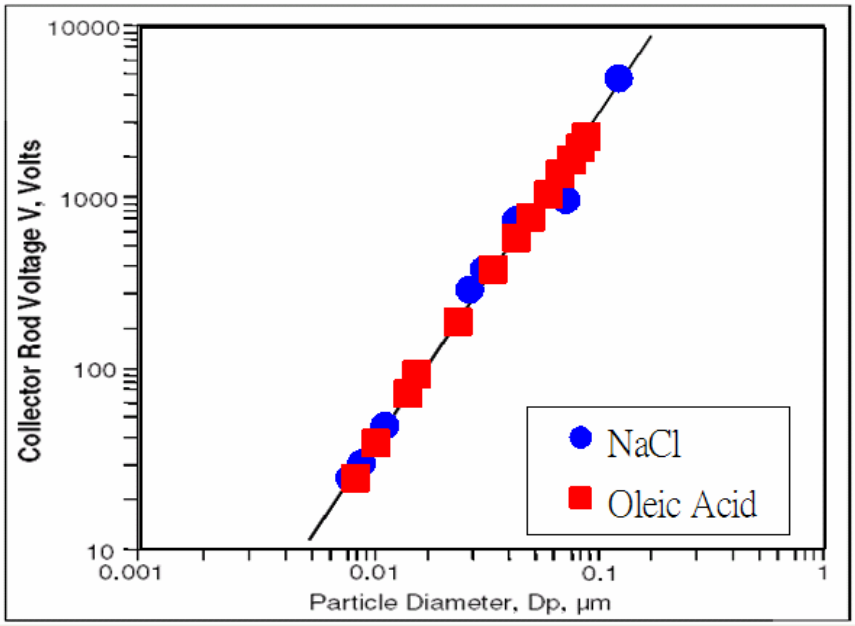

Fig. 7. Relationship between the diameter of monodisperse particles and the voltage of DMA.

Table 10. Comparison between experimental and theoretical diameters of monodisperse oleic acid droplets.

d_d-exp (nm)	92.5	85.9	78.41	70.5	61.7	52.1
C_m(g/cm^3)	8.88×10^{-12}	1.28×10^{-11}	1.87×10^{-11}	2.73×10^{-11}	3.34×10^{-11}	3.36×10^{-11}
ρ_L (g/cm^3)	0.894	0.894	0.894	0.894	0.894	0.894
N (#/cm^3)	2.4×10^4	4.3×10^4	8.2×10^4	1.65×10^5	2.99×10^5	5.0×10^5
d_d-cal (nm)	92.460	85.994	78.686	70.705	62.027	52.361
Percent discrepancy (%)	0.04%	-0.11%	-0.35%	-0.29%	-0.53%	-0.50%
d_d-exp (nm)	44.6	36.1	25.2	15	11	8.9
C_m (g/cm^3)	2.67×10^{-11}	1.76×10^{-11}	4.71×10^{-11}	4.92×10^{-11}	7.66×10^{-11}	9.98×10^{-15}
ρ_L (g/cm^3)	0.894	0.894	0.894	0.894	0.894	0.894
N (#/cm^3)	6.40×10^5	7.60×10^5	6.20×10^5	3.10×10^5	1.21×10^5	3.0×10^5
d_d-cal (nm)	44.668	36.710	25.318	15.023	11.059	8.924
Percent discrepancy (%)	-0.15%	-1.66%	-0.47%	-0.15%	-0.53%	-0.27%

Note: Furnace temperature: 240℃, Carrier gas flow rate: 0.7 L/min

CONCLUSIONS

In the generation of polydisperse particles, the CMD and GSD vary as $NaCl_{(aq)}$ concentration varies. The R^2 values show that $NaCl_{(aq)}$ concentration plays a significant role in the generation process. For generation of polydisperse oleic acid particles, the variation of GSD relates to furnace temperature and carrier gas flow rate, and they are linear relations. GSD also increases as furnace temperature or carrier gas flow rate increases. The relation is also linear between carrier gas flow rate and CMD. However, the experimental relation of furnace temperature and CMD is a polynomial function.

The main purpose of this study was to generate test nanoparticles and qualify their GSD as monodisperse aerosol. The CMD and GSD of monodisperse NaCl particles generated by atomization method were from 8.33 to 128 nm and 1.04 to 1.08, respectively. NC was from 9.89 $\times 10^2$ to 2.67 $\times 10^5$ #/cm^3. On the other hand, the CMD and GSD of monodisperse oleic acid particles generated by tube-furnace method were from 8.9 to 92.5 nm and 1.04 to 1.06, respectively. NC was from 2.4 $\times 10^4$ to 7.6 $\times 10^5$ #/cm^3. In comparing experimental theoretical values, the discrepancies for polydisperse NaCl particles resulted from the accumulation of solvent impurity on the solid particles, which caused larger particles than expected. On the discrepancies in polydisperse oleic acid particles, the furnace temperatures and carrier gas flow rates showed significant effects on both experimental data and theoretical values because they affected the amount of vapor generation.

During the process of generating these particles, several important factors which affect the transformation, transportation, and loss of aerosols should be further studied in the future. These include: aerosol aggregation in high concentration, diffusion loss of ultrafine particles, evaporation loss of ultrafine droplets, deposition of charged particles, and the solution impurity.

REFERENCES

Altmann, J., and Peters, C. (1992). The Adjustment of the Particle Size at a Sinclair-La Mer-Type Aerosol Generator, *J. Aerosol Sci.* 23 (Supplement 1): S277-S280.

Baron, P.A., and Willeke, K. (2001). *Aerosol Measurement: Principles Techniques and Applications, 2nd ed.*, A John Wiley & Sons, Inc., New York.

Chen, D.R., Pui D.Y.H., and Kaufman S.L. (1995). Electrospraying of Conducting Liquids for Monodisperse Aerosol Generation in the 4 nm to 1.8 μm Diameter Range*, J. Aerosol Sci.* 26: 963-977.

Chen, T.M., and Chein, H.M. (2003). *Nanoparticle Generation and Monitoring Technology – Efficient Testing Application of Control and Protection Equipments*, 1st Ed., ITRI, Hsinchu, 14-77.

Deppert, K., Bovin, J.O., Malm, J.O., and Samuelson, L. (1996). A New Method to Fabricate Size-selected Compound Semiconductor Nanocrystals: Aerotaxy. *J. Crystal Growth* 169: 13-19.

Flagan, R.C. (1998). History of Electrical Aerosol Measurements, *Aerosol Sci. Technol.* 28: 301–380.

Hinds, W. (1999). *Aerosol Technology: Properties, Behavior, and Measurement of Airborne Particles*, 2_{nd} ed., A John Wiley & Sons, Inc., New York.

Kruis, F.E., Goossens, A., and Fissan, H. (1996). Synthesis of Semiconducting nanoparticles. *J. Aerosol Sci.* 27, S1: 165-166.

Kruis, F.E., Fissan, H., and Peled. A. (1998). Synthesis of Nanoparticles in the Gas Phase for Electronic, Optical and Magnetic Applications: a Review, *J. Aerosol Sci.* 29(5/6): 511-535,

Liu, B.Y.H., and Lee, K.W. (1975). An Aerosol Generator of High Stability, *Am. Ind. Hyg. Assoc. J.* 36: 861-865.

Remiarz, R.J., Agarwal, J.K., and Johnson, E.M. (1982). Improved Polystyrene Latex and Vibrating Orifice Monodisperse Aerosol Generators, *TSI Quarterly.* VIII(3): 3-12.

Rader, D.J., and McMurry, P.H. (1986). Application of the Tandem Differential Mobility Analyzer to Studies of Droplet Growth or Evaporation, *J. Aerosol Sci.* 17: 771.

Rulison, A.J., and Flagan, R.C. (1994). Electrospray Atomization of Electrolytic Solutions, *Journal of Colloid and Interface Science* 167(1): 135-145.

Seola, K.S. (2002). A differential mobility analyzer with adjusTable column length for wide particle-size-range measurements, *J. Aerosol Sci.* 33: 1481–1492.

TSI Inc. (2002). *Model 3075/3076 Constant Output Atomizer: Instruction Manual*, TSI Inc., USA.

Takahashi, K. (1989). *Principle of Aerosol Science*, *2_{nd} ed.,* Fuhan, Tainan, pp.169-191.

Websites: http://www.tsi.com/; http://www.palas.de; http://www.topas-gmbh.de

Zachariah, M.R., Aquino, M.I., Shull, R.D., and Steel, E.B. (1995). Formation of Superparamagnetic Nanocomposites from Vapor Phase Condensation in a Fame. *Nanostructure. Materials*. 5, 383-392.

Received for review, August 3, 2005

Accepted, July 27, 2006